

---

# CMS Physics Analysis Summary

---

Contact: cms-pag-conveners-higgs@cern.ch

2011/12/13

## Combination of CMS searches for a Standard Model Higgs boson

The CMS Collaboration

### Abstract

The combination of results of searches for a Standard Model Higgs boson in five decay modes ( $\gamma\gamma$ ,  $bb$ ,  $\tau\tau$ ,  $WW$ , and  $ZZ$ ) performed by the CMS Collaboration at the Large Hadron Collider, CERN, is presented. The search is performed for Higgs boson masses in the range of 110–600  $\text{GeV}/c^2$ . The data correspond to an integrated total luminosity of up to  $4.7 \text{ fb}^{-1}$  of proton-proton collisions at  $\sqrt{s} = 7 \text{ TeV}$ . The expected exclusion range in the absence of the Standard Model Higgs boson is 117–543  $\text{GeV}/c^2$  at 95% C.L. The observed data allow us to exclude the Standard Model Higgs boson in the mass range 127–600  $\text{GeV}/c^2$  at 95% C.L. At 99% C.L., we exclude the SM Higgs boson in the mass range from 128–525  $\text{GeV}/c^2$ . The excess of events observed for hypothesised Higgs boson masses at the low end of the explored range makes the observed limits weaker than expected. To ascertain the origin of this excess, more data are required.



## 1 Introduction

The discovery of the mechanism for electroweak symmetry breaking is one of the key parts of the physics program at the Large Hadron Collider (LHC). In the Standard Model (SM), this is achieved by introducing a complex scalar doublet, leading to spontaneous electroweak symmetry breaking and the prediction of the Higgs boson ( $H$ ) [1–6]. In the simplest realization of the model, the mass of the Higgs boson is the only unknown, all other parameters being reasonably well constrained by existing measurements. To date, the experimental searches for this elusive particle have yielded negative results, and limits on its mass have been placed by experiments at LEP,  $m_H > 114.4 \text{ GeV}/c^2$  [7], the Tevatron,  $m_H \notin [100, 108]$  and  $m_H \notin [156, 177] \text{ GeV}/c^2$  [8], and LHC  $m_H \notin [141, 476] \text{ GeV}/c^2$  [9]. All limits quoted in this note are at 95% C.L. unless explicitly stated otherwise. The Tevatron and LHC results are preliminary. Fits of the electroweak precision measurements, not taking into account the direct search results, constrain indirectly the SM Higgs boson mass to be relatively light,  $m_H < 158 \text{ GeV}/c^2$  [10].

In this Letter, we report on the overall combination of Higgs boson searches in five decay modes ( $\gamma\gamma$ ,  $bb$ ,  $\tau\tau$ ,  $WW$ , and  $ZZ$ ) carried out by the CMS Collaboration [11]. Each of these analyses has a number of independent sub-channels adding up to a total of 42 exclusive signatures in the overall combination.

The cross sections for each Higgs boson production mechanism, together with their uncertainties, and the Higgs decay branching ratios are taken from the LHC Higgs Cross Section Group report [12]. The  $gg$ -fusion cross section is calculated at NNLO<sub>QCD</sub> + NNLL<sub>QCD</sub> + NLO<sub>EWK</sub> precision, the vector boson fusion (VBF) and the associated  $WH$  and  $ZH$  cross sections at NNLO<sub>QCD</sub> + NLO<sub>EWK</sub> precision, and  $t\bar{t}H$  at NLO<sub>QCD</sub> precision.

## 2 Searches entering the combination

Table 1 lists individual analyses used in the combination and summarizes some of their main characteristics: mass range of the search, integrated luminosity used, number of exclusive final states, and relative mass resolution.

The  $H \rightarrow \gamma\gamma$  analysis [13] is a search for a narrow peak in the di-photon mass distribution. All events are split into four categories based on whether both photons are in the central part of the CMS detector and whether both photons have produced compact electromagnetic showers. This is motivated by the differences in the photon energy resolutions of the barrel/endcap electromagnetic calorimeters and for photons showering or non-showering in the detector volume

Table 1: Summary information on the analyses included in the combination ( $\ell = e, \mu$ ).

Channel	$m_H$ range (GeV/ $c^2$ )	Lumi (fb $^{-1}$ )	sub- channels	$m_H$ reso- lution
$H \rightarrow \gamma\gamma$	110 – 150	4.7	4	1–3%
$H \rightarrow \tau\tau$	110 – 145	4.6	9	20%
$H \rightarrow bb$	110 – 135	4.7	5	10%
$H \rightarrow WW \rightarrow \ell\nu\ell\nu$	110 – 600	4.6	5	20%
$H \rightarrow ZZ \rightarrow 4\ell$	110 – 600	4.7	3	1–2%
$H \rightarrow ZZ \rightarrow 2\ell 2\tau$	190 – 600	4.7	8	10–15%
$H \rightarrow ZZ \rightarrow 2\ell 2\nu$	250 – 600	4.6	2	7%
$H \rightarrow ZZ \rightarrow 2\ell 2q$	$\left\{ \begin{array}{l} 130 – 164 \\ 200 – 600 \end{array} \right.$	4.6	6	3%

before the electromagnetic calorimeters. The di-photon mass resolution varies from 1%–3%, depending on the category. The background under the expected signal peak is derived from sidebands.

The  $H \rightarrow bb$  search [14] relies on Higgs boson production in association with  $W$  or  $Z$  bosons ( $V$ ). We use the following  $W$  and  $Z$  boson decay modes:  $W \rightarrow e\nu/\mu\nu$  and  $Z \rightarrow ee/\mu\mu/\nu\nu$ . The presence of neutrinos is tagged by requiring a missing transverse energy  $E_T^{\text{mis}}$  defined as a vector opposite to the vector sum of transverse momenta of all reconstructed objects in the volume of the detector (leptons, photons, and charged/neutral hadrons). The dijet system, with both jets being  $b$ -tagged, is required to be boosted in the transverse plane, which helps reduce backgrounds and improve the dijet mass resolution to about 10%. The main backgrounds  $V$ +jets,  $Vb\bar{b}$ , and  $t\bar{t}$  are derived from data control samples. The  $WZ$  and  $ZZ$  backgrounds with a  $Z$  boson decaying to  $b\bar{b}$  as well as the single top background are predicted via simulation. In this search, we use a Multivariate Analysis (MVA) technique. A cut is placed on the MVA output and we count the number of events passing the cut in the five channels.

The  $H \rightarrow \tau\tau$  search [15] is performed using the di-tau final state signatures  $e\mu$ ,  $e\tau_h$ ,  $\mu\tau_h$ , where  $\tau_h$  stands for a  $\tau$  decaying hadronically. Each of these three categories is further divided into exclusive sub-categories according to the associated jet activity: events with two VBF-like jets (two forward/backward leading jets with no jets in between), events with exactly one high  $E_T$  jet, and events with no or exactly one low  $E_T$  jet. The total number of exclusive channels is therefore nine. In each of these nine categories we search for a broad excess in the di-tau mass  $m_{\tau\tau}$  distribution. The expected Higgs boson mass resolution is about 20%. The main irreducible background is  $Z \rightarrow \tau\tau$ . Its  $m_{\tau\tau}$  distribution is derived from data by using  $Z \rightarrow \mu\mu$  events, in which the reconstructed muons are replaced with reconstructed particles from the decay of simulated taus with the same momentum. The reducible backgrounds ( $W$  + jets, QCD,  $Z \rightarrow ee$ ) are evaluated using data driven techniques.

In the  $H \rightarrow WW \rightarrow 2\ell 2\nu$  search [16], we look for an excess of events with two leptons of opposite sign, missing transverse energy, and 0/1/2 jets. All events are split into five categories, which is largely motivated by the different background compositions and signal-to-background ratios. For events with 0 jets, the main background is electroweak  $WW$  production. For events with 1 jet,  $WW$  and  $t\bar{t}$  are the main backgrounds. Both 0- and 1-jet categories are further split into same-flavour and opposite-flavour dilepton sub-channels, since the Drell-Yan background is much larger for the same-flavour dilepton events. The 2-jet category is optimized to take advantage of the VBF production signature. The main background for this channel is  $t\bar{t}$ . We use a MVA technique in which the MVA is trained for a number of discrete Higgs boson mass points; and we search for an excess of events in the MVA output distributions. Due to the presence of the two neutrinos in the final states, the mass resolution in this channel is about 20%. All backgrounds, except for very small contributions from  $WZ$ ,  $ZZ$ , and  $W\gamma$  are evaluated directly from data using various control samples.

In the  $H \rightarrow ZZ \rightarrow 4\ell$  search [17], we look for a four-lepton mass peak over the continuum background. The  $4e$ ,  $4\mu$ ,  $2e2\mu$  sub-channels are tracked individually, as there are differences in the four-lepton mass resolutions that typically range from 1% - 2%, depending on the Higgs boson mass and the final state. For Higgs boson masses above 250 GeV/ $c^2$ , the instrumental four-lepton mass resolution becomes smaller than the intrinsic total width of the Higgs boson. The dominant irreducible background is electroweak  $ZZ$  diboson production (with both  $Z$ s decaying to either  $2e$ ,  $2\mu$ , or  $2\tau$ ) and taken from simulation. The smaller backgrounds with jets faking leptons (e.g.  $Z$  + jets,  $Zb\bar{b}$ ,  $t\bar{t}$ ) are evaluated all together from data.

In the  $H \rightarrow ZZ \rightarrow 2\ell 2\tau$  search [18], one  $Z$  boson is required to decay to a dilepton pair ( $e^+e^-$

or  $\mu^+\mu^-$ ) forming an on-shell  $Z$  boson. The other  $Z$  boson is required to decay to  $\tau\tau$ , with the following four final state signatures used in the analysis:  $e\mu$ ,  $e\tau_h$ ,  $\mu\tau_h$ ,  $\tau_h\tau_h$ . Overall, this makes eight exclusive final sub-channels. We search for a broad excess in the visible mass distribution, where the visible (invariant) mass is constructed from the visible  $\tau$ -decay products, without an attempt to account for missing neutrinos. Due to the presence of neutrinos, the Higgs boson mass resolution in this analysis is about 10–15%. The dominant background is electroweak  $ZZ$  diboson production and taken from simulation. The main sub-leading backgrounds with jets faking  $\tau$ -leptons come from  $Z + \text{jets}$  (including  $ZW$ ) and  $t\bar{t}$ . These backgrounds are evaluated all together using data driven techniques.

In the  $H \rightarrow ZZ \rightarrow 2\ell 2\nu$  search [19], we select events with a dilepton pair ( $e^+e^-$  or  $\mu^+\mu^-$ ), requiring their invariant mass be consistent with an on-shell  $Z$  boson, and a large missing transverse energy  $E_T^{\text{mis}}$ . We then build the transverse invariant mass  $m_T$  from the dilepton pair momenta and  $E_T^{\text{mis}}$ , assuming that  $E_T^{\text{mis}}$  arises from a  $Z \rightarrow \nu\nu$  decay. We search for a correspondingly broad excess of events in the  $m_T$  distribution. The  $m_T$  observable carries information on the Higgs boson mass with a mass resolution of about 7%. The  $ZZ$  and  $WZ$  backgrounds are taken from simulation, while all other backgrounds,  $Z + \text{jets}$  and a cumulative sum of the rest, are evaluated from control samples in data.

In the  $H \rightarrow ZZ \rightarrow 2\ell 2q$  search [20], we select events with two leptons ( $e^+e^-$  or  $\mu^+\mu^-$ ) and two jets with two, one, or no  $b$ -tags, which makes a total of six exclusive final states. Motivation for  $b$ -tagging is driven by the high rate of  $b$ -jets in  $Z \rightarrow q\bar{q}$  decays in comparison to general QCD jets produced in association with a  $Z$  boson. The two jets are required to form an invariant mass consistent with the  $Z$  boson mass taking into account the dijet mass resolution. For the search in the mass range 200–600  $\text{GeV}/c^2$ , the mass of the dilepton pair is also required to be consistent with the  $Z$  boson mass. For the search in the mass range 130–164  $\text{GeV}/c^2$ , the requirement on the mass of the dilepton pair is relaxed. In the high mass range, events are further selected using a cut on a multivariate angular likelihood constructed from the kinematic variables of the two leptons and two jets. In this search we look for a peak in the dilepton-dijet invariant mass distribution, with the dijet mass constrained to the mass of the  $Z$  boson. The mass resolution in this search is about 3%. The background dilepton-dijet mass distribution is derived using control regions in data.

### 3 Combination methodology

For calculations of exclusion limits, we use the modified frequentist construction  $\text{CL}_s$  [21, 22]. To fully define the method, one needs to make a choice of test statistic and of treatment of the systematic uncertainties in the construction of the test statistic and in generating pseudo-data. In this Letter, we follow the LHC Higgs Combination Group prescription [23].

As the first step, we account for all independent sources of systematic uncertainties, both theoretical and instrumental, and assign each of them its own nuisance parameter  $\theta_i$ , whose best estimate, prior to analyzing data entering the combination, is  $\tilde{\theta}_i$ . Any given nuisance parameter may affect the signal and background rate in multiple channels. The scale of the effect need not be identical; positive and negative correlations are also allowed. Following the frequentist paradigm, the  $\tilde{\theta}_i$  values are treated as arising from some *real* or *imaginary* measurements of the nuisance parameters. The probability of “measuring”  $\tilde{\theta}_i$ , given the true value  $\theta_i$ , is  $p_i(\tilde{\theta}_i | \theta_i)$  and describes the scale of the systematic uncertainties. In this combination, the probability  $p_i(\tilde{\theta}_i | \theta_i)$  can be one of the following three kinds: *uniform* for uncertainties not constrained by anything except for the data directly used in the combination; *Poisson* for uncertainties associated with statistical errors in measuring event counts in control regions (in this case,  $\tilde{\theta}_i$  is the observed

number of events in the control region); *normal* for all other uncertainties. When a nuisance parameter is taken to be distributed according to the normal *pdf*, the effect of its variation on an observable  $\mathcal{O}$  is propagated either as a Gaussian error,  $\mathcal{O} = \mathcal{O}_0 \cdot (1 + \sigma \cdot \theta)$ , or as a log-normal error,  $\mathcal{O} = \mathcal{O}_0 \cdot \kappa^\theta$ , where  $\sigma$  and  $\kappa$  characterize the relative scale of the uncertainties. The former choice is used for observables that can take both negative and positive values, while the latter option is used for positive definite observables. The total number of nuisance parameters tracked in the combination depends on the Higgs boson mass and ranges from 156 to 222.

The likelihood  $\mathcal{L}(\text{data} | \mu, \theta)$  to be used in constructing the test statistic is defined as:

$$\mathcal{L}(\text{data} | \mu, \theta) = \text{Poisson}(\text{data} | \mu \cdot s(\theta) + b(\theta)) \cdot p(\tilde{\theta} | \theta), \quad (1)$$

where  $\text{Poisson}(\text{data} | \mu s(\theta) + b(\theta))$  is the Poisson probability to observe data, assuming the expected signal and background models,  $s(\theta)$  and  $b(\theta)$ , that in general depend on some nuisance parameters  $\theta$ . The free parameter  $\mu$  is a common signal strength modifier affecting signal event yields in all production modes.

The test statistic is then defined as the profile likelihood ratio, given by:

$$q_\mu = -2 \ln \frac{\mathcal{L}(\text{data} | \mu, \hat{\theta}_\mu)}{\mathcal{L}(\text{data} | \hat{\mu}, \hat{\theta})}, \text{ with a constraint } 0 \leq \hat{\mu} \leq \mu \quad (2)$$

where *data* can be the actual *experimental observation* or *pseudo-data*, generated for the purposes of building expected sampling distributions for the test statistic. Both the denominator and numerator are maximized. In the numerator,  $\mu$  remains fixed and only the nuisance parameters  $\theta$  are allowed to float. Their values at which  $\mathcal{L}$  reaches the maximum are denoted as  $\hat{\theta}_\mu$ . In the denominator, both  $\mu$  and  $\theta$  are allowed to float in the fit, and  $\hat{\mu}$  and  $\hat{\theta}$  are parameters at which  $\mathcal{L}$  reaches its global maximum. The lower constraint on  $\hat{\mu}$  ( $0 \leq \hat{\mu}$ ) is imposed by hand as the signal rate cannot be negative. The upper constraint ( $\hat{\mu} \leq \mu$ ) forces the limit to be one-sided. For observations preferring the best-fit values of  $\hat{\mu} > \mu$ , the test statistic is set to zero. The value of the test statistic for the actual *observation* will be denoted as  $q_\mu^{\text{obs}}$ .

Next, we find the values of the nuisance parameters  $\hat{\theta}_0^{\text{obs}}$  and  $\hat{\theta}_\mu^{\text{obs}}$  best describing the experimentally *observed* data (i.e. maximizing  $\mathcal{L}$ ), for the *background-only* and *signal+background* hypotheses, respectively. Using these best-fit values of the nuisance parameters, we generate toy Monte Carlo pseudo-data sets to construct the test statistic sampling distributions for the *signal+background* hypothesis (assuming a signal with strength  $\mu$ ) and for the *background-only* hypothesis ( $\mu = 0$ ). The ‘‘measurements’’  $\tilde{\theta}$  are also randomized in each pseudo-data, using their *pdfs*  $p(\tilde{\theta} | \theta)$ . Note, that for the purposes of pseudo-data generation, the nuisance parameters are fixed to their data-driven best-fit values  $\hat{\theta}_\mu^{\text{obs}}$  or  $\hat{\theta}_0^{\text{obs}}$ , but are allowed to float in fits needed to evaluate the test statistic.

Having constructed the *signal+background* and *background-only* sampling distributions for the test statistic  $q_\mu$ , we find two tail probabilities to be associated with the actual observation; namely, the probability to obtain a test statistic value as high as, or higher than, the one observed in data, under the *signal+background* hypothesis:

$$P\left(q_\mu \geq q_\mu^{\text{obs}} \mid \mu s(\hat{\theta}_\mu^{\text{obs}}) + b(\hat{\theta}_\mu^{\text{obs}})\right), \quad (3)$$

and under the *background-only* hypothesis:

$$P\left(q_\mu \geq q_\mu^{\text{obs}} \mid b(\hat{\theta}_0^{\text{obs}})\right). \quad (4)$$

Then, we calculate  $CL_s(\mu)$  as a ratio of these two tail probabilities,

$$CL_s(\mu) = \frac{P\left(q_\mu \geq q_\mu^{obs} \mid \mu_S(\hat{\theta}_\mu^{obs}) + b(\hat{\theta}_\mu^{obs})\right)}{P\left(q_\mu \geq q_\mu^{obs} \mid b(\hat{\theta}_0^{obs})\right)}. \quad (5)$$

If  $CL_s \leq \alpha$  for  $\mu = 1$ , we say that the SM Higgs boson is excluded at the  $(1 - \alpha)$  confidence level. To quote the 95% confidence level upper limit on  $\mu$ , we adjust  $\mu$  until we reach  $CL_s = 0.05$ . The  $CL_s$  method gives conservative limits, i.e. the actual confidence level is higher than  $(1 - \alpha)$ .

To quantify an excess of events, we use the alternative test statistic  $q_0$ , defined as follows:

$$q_0 = -2 \ln \frac{\mathcal{L}(\text{data} \mid 0, \hat{\theta}_0)}{\mathcal{L}(\text{data} \mid \hat{\mu}, \hat{\theta})} \quad \text{and} \quad \hat{\mu} \geq 0. \quad (6)$$

This test statistic allows us to evaluate significances ( $Z$ ) and  $p$ -values ( $p_0$ ) from the following asymptotic formula [24]:

$$Z = \sqrt{q_0^{obs}}, \quad (7)$$

$$p_0 = P(q_0 \geq q_0^{obs}) = \frac{1}{2} \left[ 1 - \text{erf}\left(Z/\sqrt{2}\right) \right], \quad (8)$$

where  $q_0^{obs}$  is the observed test statistic calculated for  $\mu = 0$  and with only one constraint  $0 \leq \hat{\mu}$ , which ensures that data deficits are not counted on an equal footing with data excesses.

## 4 Results

Figure 1 shows the  $CL_s$  value for the SM Higgs boson as a function of its mass. The observed values are shown by the solid line. The dashed line indicates the median expected value of  $CL_s$ , while the green and yellow bands indicate the  $\pm 1\sigma$  (68%) and  $\pm 2\sigma$  (95%) ranges in which the observed results are expected to reside for the *background-only* hypothesis. The red horizontal lines indicate  $CL_s$  values of 0.01, 0.05, and 0.10. The mass regions where the observed  $CL_s$  values are below these lines are excluded with the corresponding  $1 - CL_s$  confidence levels: 99%, 95%, and 90%.

We exclude the SM Higgs boson at 95% C.L. in the mass range 127–600 GeV/ $c^2$ . At 99% C.L., we exclude the SM Higgs boson in the mass range from 128–525 GeV/ $c^2$ . Given these exclusions, the allowed mass range for the SM Higgs boson is substantially reduced with respect to those coming from searches made at LEP [7], the Tevatron [8], and the recent ATLAS+CMS combined limits obtained with 1.0–2.3 fb $^{-1}$  of integrated luminosity [9].

The combined 95% C.L. upper limits on the signal strength modifier  $\mu = \sigma/\sigma_{SM}$  as a function of the Higgs boson mass are presented in Fig. 2. This plot shows by what factor the SM Higgs boson cross section must be scaled to be excluded at 95% C.L. The exclusion range for the SM Higgs boson ( $\mu = 1$ ) is identical to that shown in Fig. 1, as Figs. 1 and 2 are based on the same underlying information.

To illustrate the interplay of the individual Higgs decay modes, Fig. 3 shows the observed limits for the five decay modes studied and their combination. The limits shown are calculated using the asymptotic formula for the  $CL_s$  method [24]. For high Higgs boson masses above 200 GeV/ $c^2$ , the limits are mostly driven by the  $H \rightarrow ZZ$  decay channel. In the mass range

120–200 GeV/ $c^2$ , the limits are largely defined by the  $H \rightarrow WW$  decay mode. For the mass range below 120 GeV/ $c^2$ , the dominant contributor to the limits is  $H \rightarrow \gamma\gamma$ .

Figures 1 and 2 show that the expected exclusion, at 95% C.L., in the absence of a signal, is from 117–543 GeV/ $c^2$ . The differences between the observed and expected limits are fairly consistent with statistical fluctuations, as the observed limits are generally within the green and yellow bands.

At the highest probed Higgs boson mass range, we observe fewer events than the mean expected number, which make the observed limit somewhat stronger than the expected one. This deficit of events cannot be attributed to a single dominant channel. In the low Higgs boson mass range, we observe an excess of events. This makes the observed limits weaker than expected in the absence of the SM Higgs boson.

To quantify the consistency of the observed excesses with the background-only hypothesis, Fig. 4 (top panel) shows a scan of the observed combined local  $p$ -value (Eq. 8) in the low mass range. This scan characterizes how unlikely are the upward departures in the observed values of the test statistic  $q_0^{obs}$ . One can see that the  $p$ -value curve dips downward over a large range of masses, driven by the broad excesses in the channels with poor mass resolution, with two narrower features corresponding to the  $ZZ \rightarrow 4\ell$  and  $H \rightarrow \gamma\gamma$  channels. The first dip at  $m_H \sim 119$  GeV/ $c^2$  corresponds to three  $4\ell$  events with four-lepton mass  $m_{4\ell} \sim 119$  GeV/ $c^2$ . The second dip is mostly driven by the  $\gamma\gamma$  excess around di-photon mass  $m_{\gamma\gamma} \sim 124$  GeV/ $c^2$ .

Whilst a  $p$ -value characterizes the probability of observing a given excess of events, it does not say anything about the compatibility of the excess with the expected signal. The best-fit  $\hat{\mu}$  value is a measure of such compatibility and shown in Fig. 4 (lower panel). The blue band corresponds to the  $\pm 1\sigma$  error (statistical+systematic) on the value of  $\hat{\mu}$  as obtained in the asymptotic approximation from  $\Delta q_\mu = 1$ . One can see that the observed  $\hat{\mu}$  values are within  $1\sigma$  of 1 in nearly the entire, as yet not excluded, low mass range, i.e. the observed excess is not inconsistent with the SM Higgs boson cross section.

The minimum local  $p$ -value is  $p_{min} = 0.005$  and corresponds to a local significance of  $Z_{max} = 2.6$ , before taking into account the look-elsewhere effect [25]. The *global* significance of the excess, taking into account the look-elsewhere effect for the entire search mass range 110–600 GeV/ $c^2$ , has been approximately evaluated directly from the data following the methodology described in Ref [23] and is  $0.6\sigma$ . For a restricted range of interest, the global  $p$ -value can be evaluated by generating pseudo-data. If this is done, by way of illustration, for the mass range 110–145 GeV/ $c^2$ , we obtain a *global* significance of  $1.9\sigma$ .

Thus, while the current data have resulted in a substantially increased range of Higgs boson masses excluded at 95% C.L., they are insufficient for statistically meaningful interpretations of the observed excess of events outside of this range. More data coming in 2012 will increase the statistical accuracy of the existing analyses and allow further improvements in search strategies, enabling definitive conclusions to be drawn on the presence or absence of the SM Higgs boson in the remaining small mass window between the LEP limits and the limits presented in this Letter: 114.4–127 GeV/ $c^2$ . More data will also allow the search for the Higgs boson in the mass range above 600 GeV/ $c^2$ .

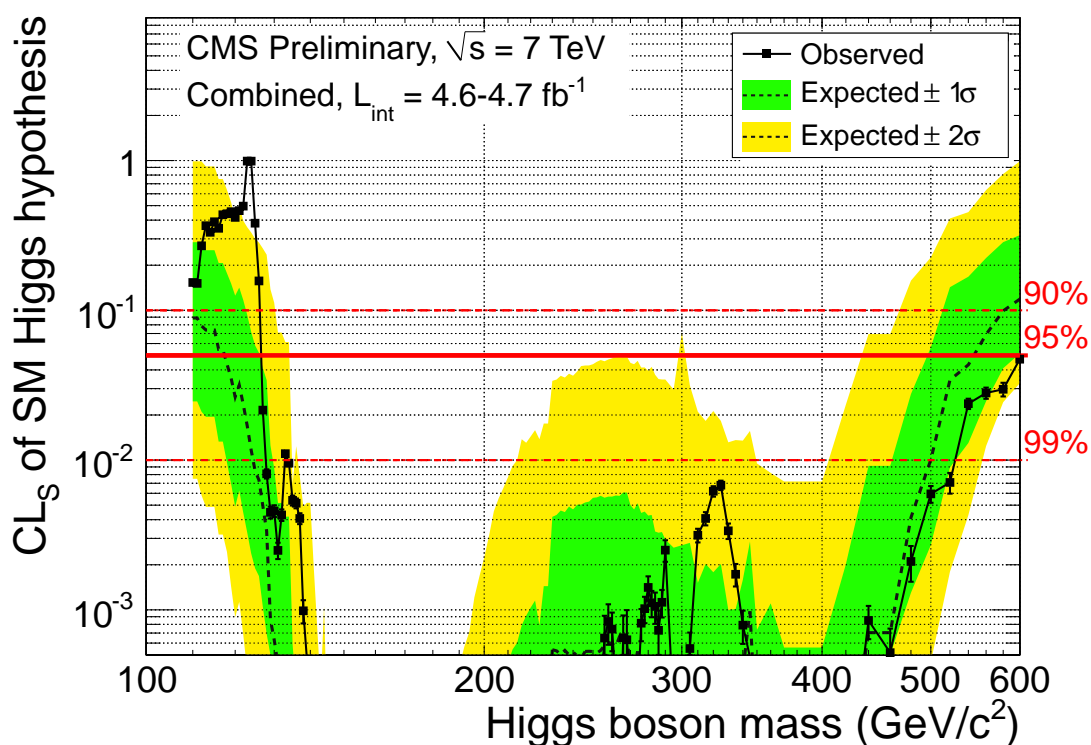


Figure 1: The  $CL_s$  value for the Standard Model Higgs boson hypothesis as a function of the Higgs boson mass in the range 110–600  $\text{GeV}/c^2$ . The observed values are shown by a solid line. The dashed black line indicates the median expected  $CL_s$  value for the background-only hypothesis, while the green (yellow) bands indicate the ranges that are expected to contain 68% (95%) of all observed limit excursions from the median. The three red horizontal lines show confidence levels of 90%, 95%, and 99% defined as  $(1 - CL_s)$ .

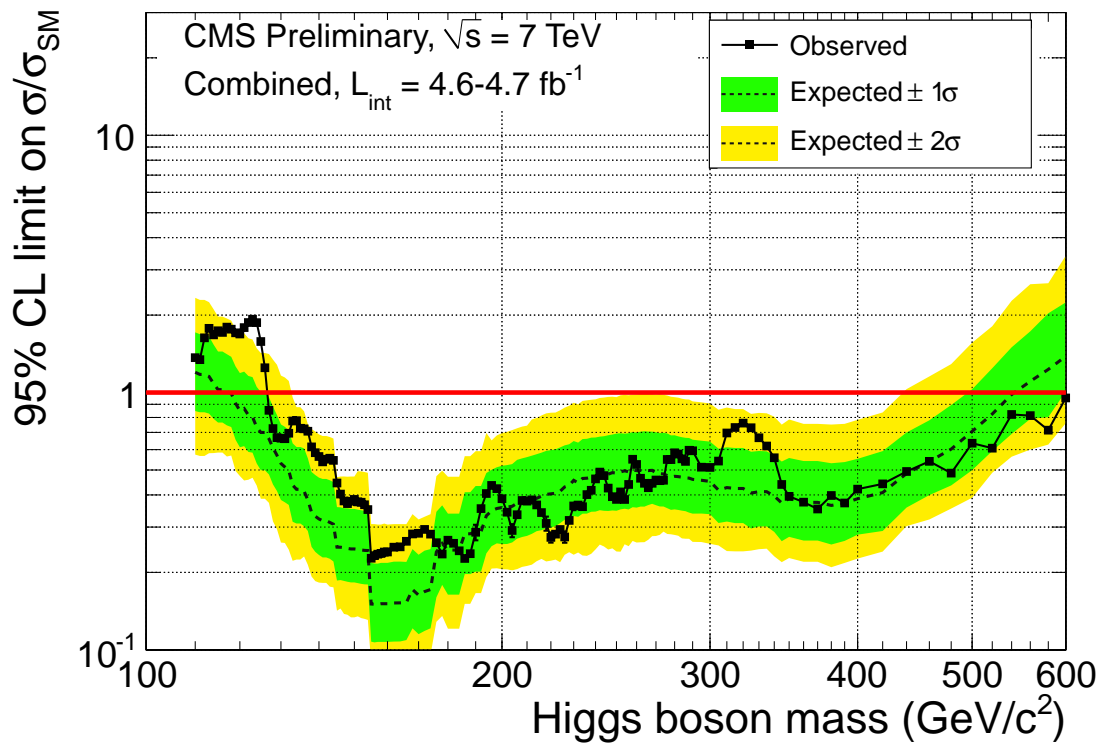


Figure 2: The combined 95% C.L. upper limits on the signal strength modifier  $\mu = \sigma/\sigma_{\text{SM}}$  as a function of the SM Higgs boson mass in the range 110–600 GeV/ $c^2$ . The observed limits are shown by the solid symbols and the black line. The dashed line indicates the median expected limit on  $\mu$  for the background-only hypothesis, while the green (yellow) bands indicate the ranges that are expected to contain 68% (95%) of all observed limit excursions from the median.

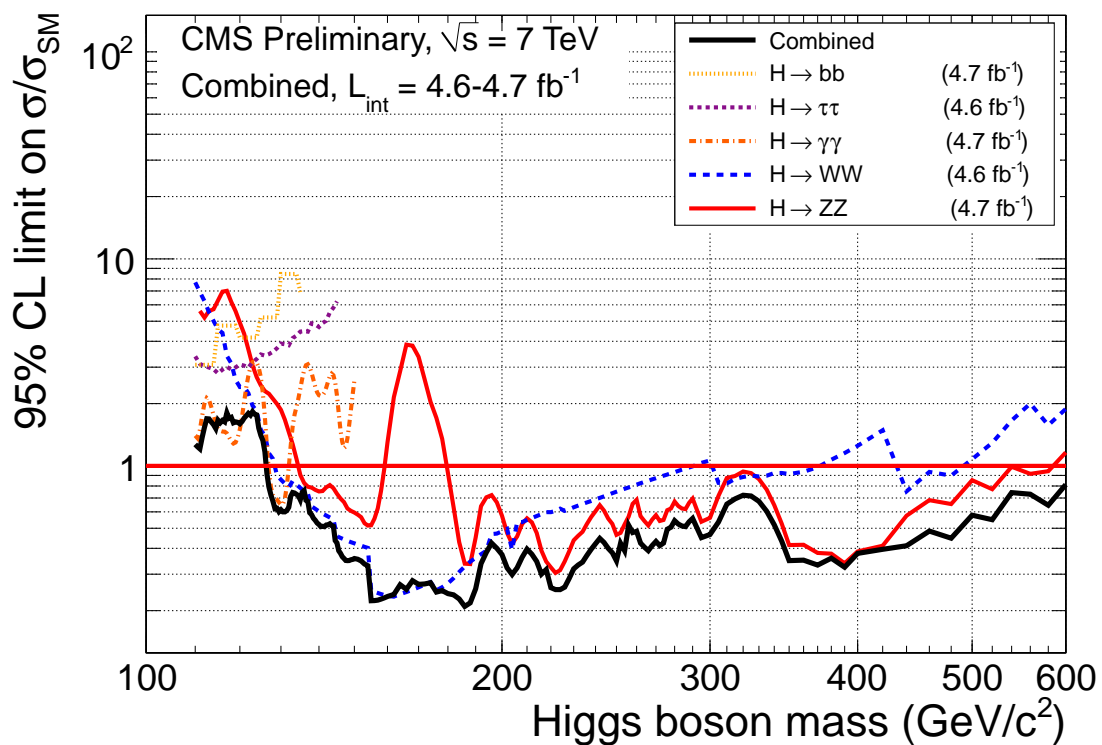


Figure 3: The observed 95% C.L. upper limits on the signal strength modifier  $\mu = \sigma/\sigma_{SM}$  as a function of the SM Higgs boson mass in the range 110–600 GeV/ $c^2$  for the five Higgs boson decay modes and their combination. The limits shown on this plot are calculated using the asymptotic formula for the CL<sub>s</sub> method [24].

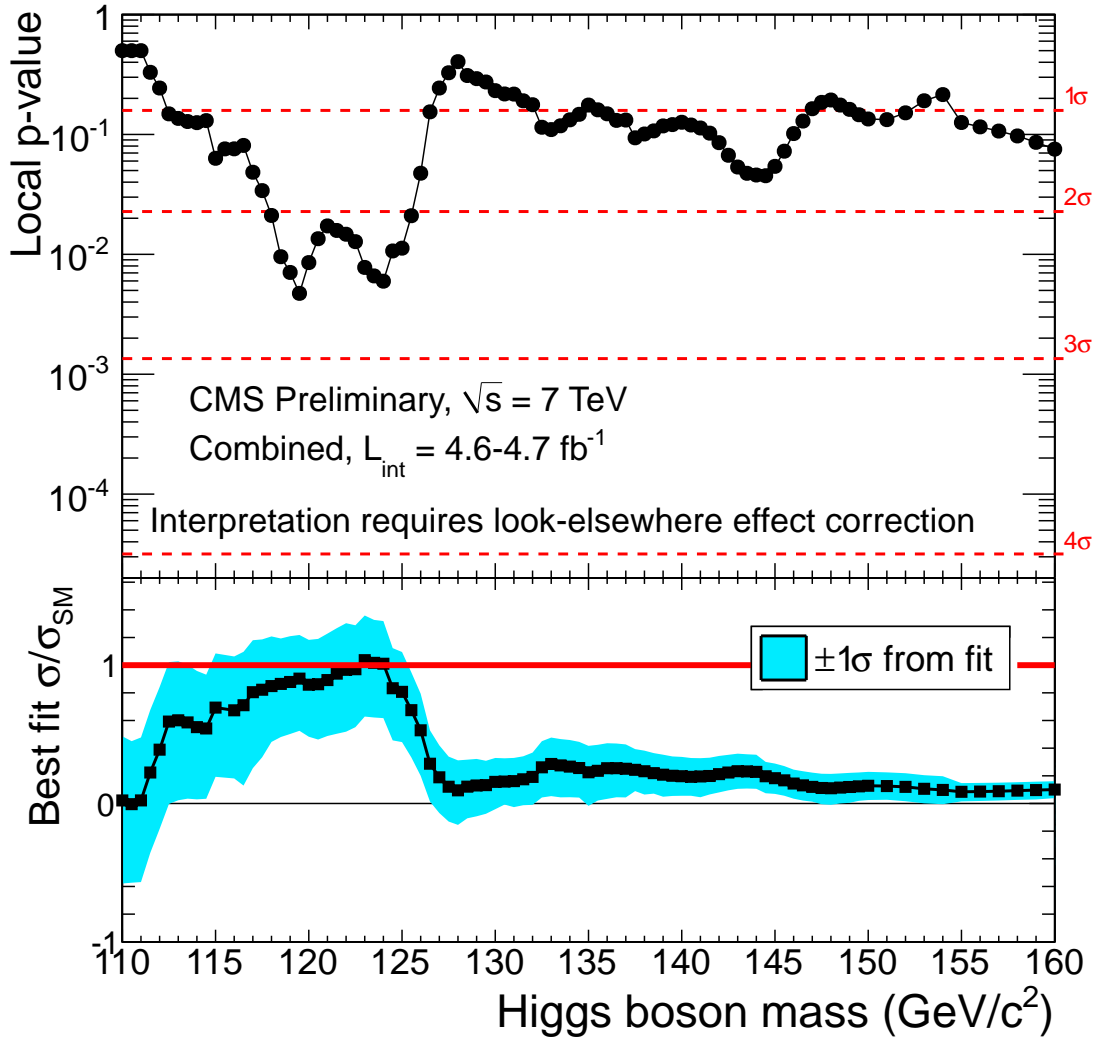


Figure 4: The observed local  $p$ -value  $p_0$  (top panel) and best-fit  $\hat{\mu} = \sigma/\sigma_{\text{SM}}$  (bottom panel) as a function of the SM Higgs boson mass in the range 110–160 GeV/ $c^2$ . The global significance of the observed maximum excess (minimum local  $p$ -value) in the mass range 110–145 GeV/ $c^2$  is about  $1.9\sigma$  as estimated by generating multiple pseudo-data sets.

---

## 5 Summary

In summary, we present the combination of results of searches for a Higgs boson in five decay modes ( $\gamma\gamma$ ,  $bb$ ,  $\tau\tau$ ,  $WW$ , and  $ZZ$ ) performed by the CMS Collaboration. The data correspond to an integrated total luminosity of up to  $4.7 \text{ fb}^{-1}$  of proton-proton collisions at  $\sqrt{s} = 7 \text{ TeV}$ . The expected exclusion range in the absence of the Standard Model Higgs boson is  $117\text{--}543 \text{ GeV}/c^2$  at 95% C.L. The observed data allow us to exclude the Standard Model Higgs boson in the mass range  $127\text{--}600 \text{ GeV}/c^2$  at 95% C.L. At 99% C.L., we exclude the SM Higgs boson in the mass range from  $128\text{--}525 \text{ GeV}/c^2$ . The excess of events observed for hypothesised Higgs boson masses at the low end of the explored range makes the observed limits weaker than expected. To ascertain the origin of this excess, more data are required.

## Appendix: Additional information

### Limits obtained with different methodologies

Figure 5 shows limits on the signal strength  $\mu$  obtained with three different methods. Filled black points show the observed  $CL_s$ -based limits, as in Fig. 2. The solid line without symbols shows limits on  $\mu$  calculated using the asymptotic formula for the  $CL_s$  method [24]. The blue open symbols are the limits obtained with the Bayesian approach [26]. The observed self-consistency of limits obtained with the two very different statistical approaches, Bayesian and modified frequentist ( $CL_s$ ), as well as the agreement of limits obtained with the CPU-intensive generation of pseudo-data and from the asymptotic analytic calculations ensure the robustness of the reported results. The  $CL_s$  and Bayesian limits on  $\mu$  are remarkably consistent for all mass points in the scan; the mean and RMS of the relative differences (Bayes- $CL_s$ )/ $CL_s$  for all mass points probed are  $-2\% \pm 5\%$  (mean  $\pm$  RMS). The differences between the asymptotic and pseudo-data based  $CL_s$  are  $-6\% \pm 4\%$  for the observed limits and  $-3\% \pm 3\%$  for the expected limits.

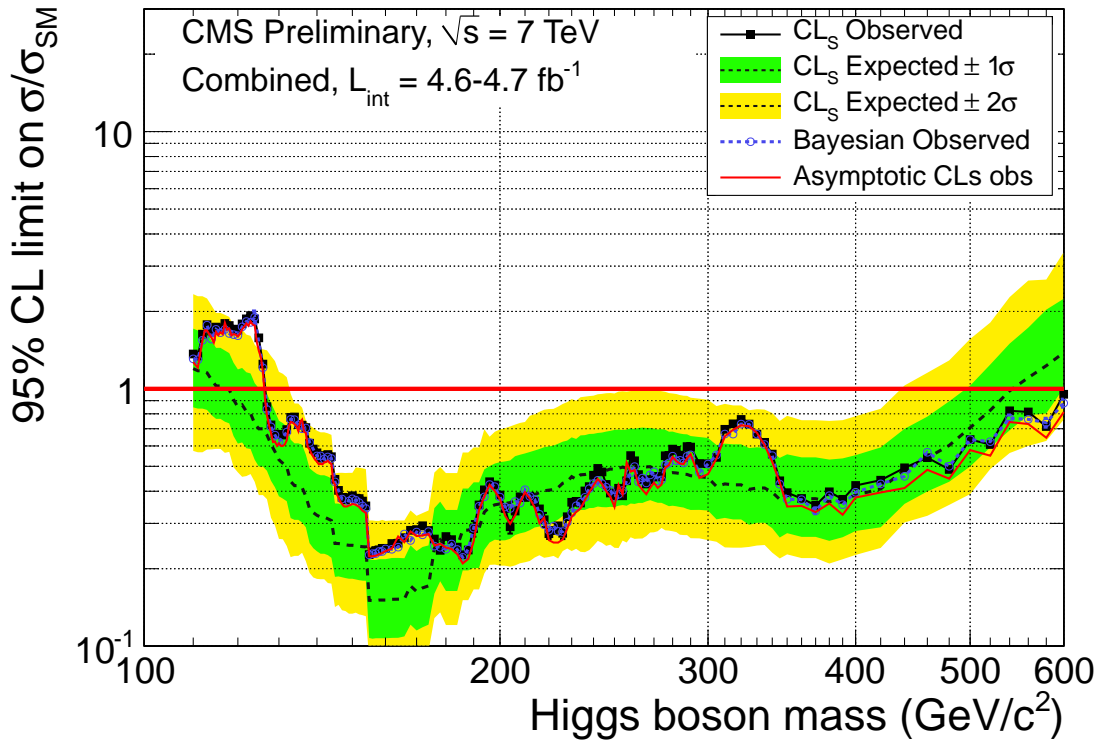


Figure 5: The observed 95% C.L. upper limits on the signal strength modifier  $\mu = \sigma/\sigma_{SM}$  as a function of the SM Higgs boson mass in the range 110-600  $\text{GeV}/c^2$  as obtained with three methods:  $CL_s$  as presented in the note (black solid points and black solid line),  $CL_s$  using an asymptotic approximation (red curve), and Bayesian (blue open circles and blue dashed line).

### Limits for all studied decay modes, without combining ZZ-subchannels

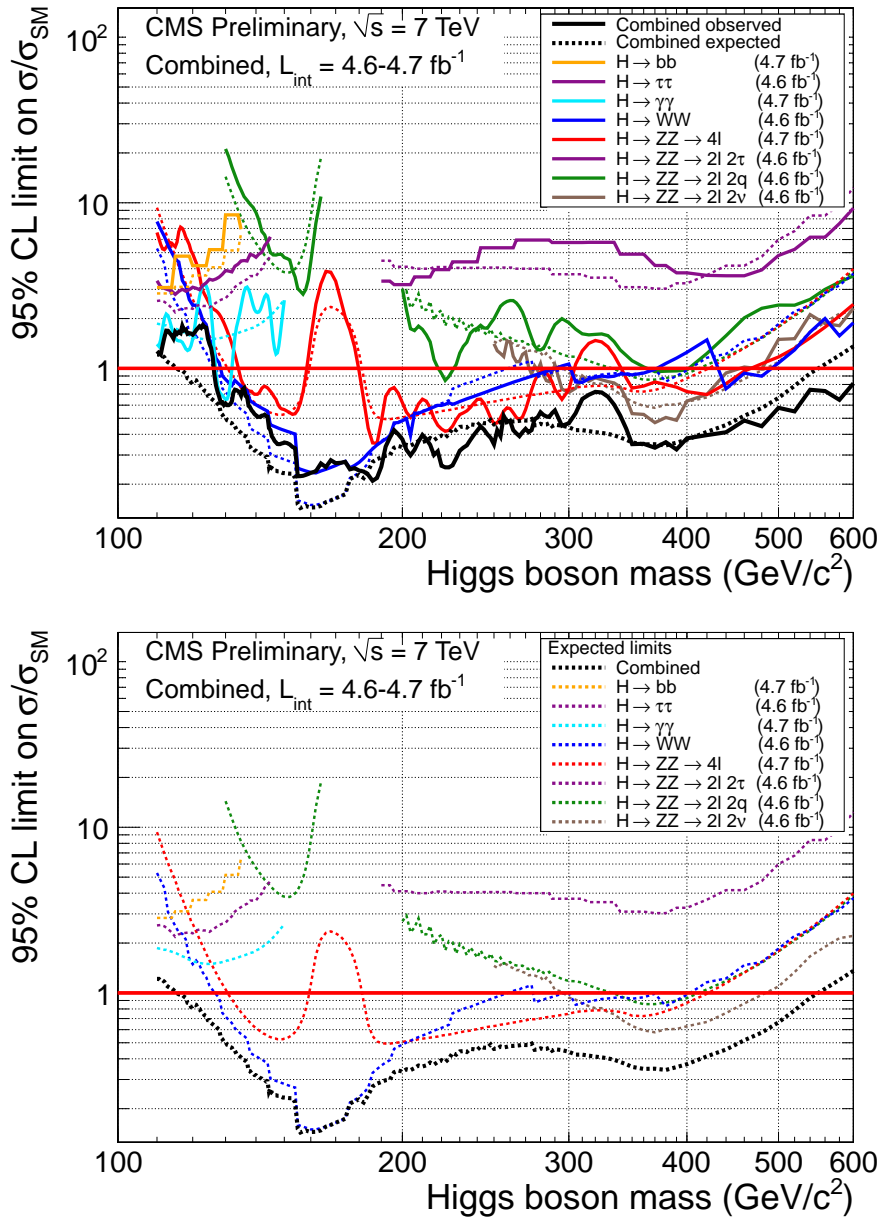


Figure 6: The observed and expected 95% C.L. upper limits on the signal strength modifier  $\mu = \sigma/\sigma_{SM}$  as a function of the SM Higgs boson mass for all eight analyses used in the combination. Solid lines are for observed limits, dashed for expected.

### Limit plots with a zoom at the low mass range

In this section, we provide zoomed versions of the limit plots, focusing on the low mass range.

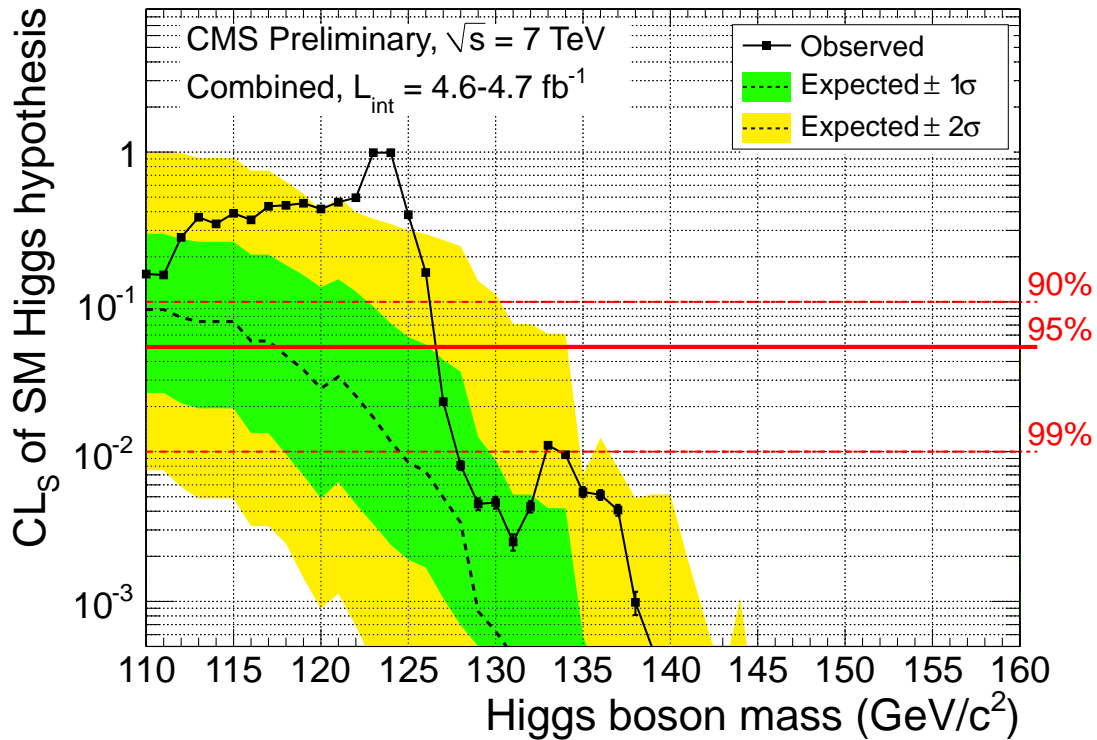


Figure 7: The  $CL_s$  value for the Standard Model Higgs boson hypothesis as a function of the Higgs boson mass in the range 110–160  $\text{GeV}/c^2$ . The observed values are shown by a solid line. The dashed black line indicates the median expected  $CL_s$  value for the background-only hypothesis, while the green (yellow) bands indicate the ranges that are expected to contain 68% (95%) of all observed limit excursions from the median. The three red horizontal lines show confidence levels of 90%, 95%, and 99% defined as  $(1 - CL_s)$ .

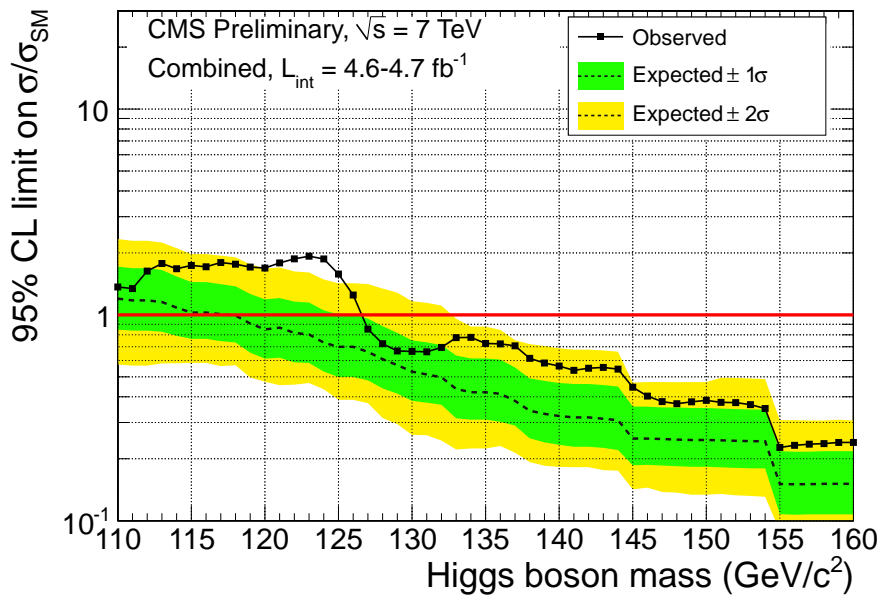


Figure 8: The combined 95% C.L. upper limits on the signal strength modifier  $\mu = \sigma/\sigma_{SM}$  as a function of the SM Higgs boson mass in the range 110–160  $\text{GeV}/c^2$ . The observed limits are shown by the solid symbols and the black line. The dashed line indicates the median expected limit on  $\mu$  for the background-only hypothesis, while the green (yellow) bands indicate the ranges that are expected to contain 68% (95%) of all observed limit excursions from the median.

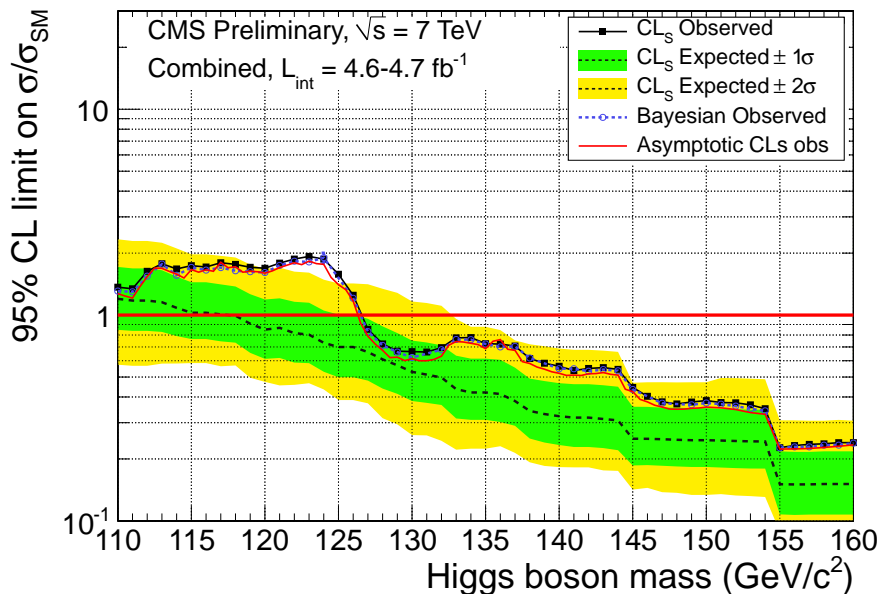


Figure 9: The observed 95% C.L. upper limits on the signal strength modifier  $\mu = \sigma/\sigma_{SM}$  as a function of the SM Higgs boson mass in the range 110–160  $\text{GeV}/c^2$  as obtained with three methods:  $CL_s$  as presented in the note (black solid points and black solid line),  $CL_s$  using an asymptotic approximation (red curve), and Bayesian (blue open circles and blue dashed line). The green (yellow) bands are the same as in Fig. 8.

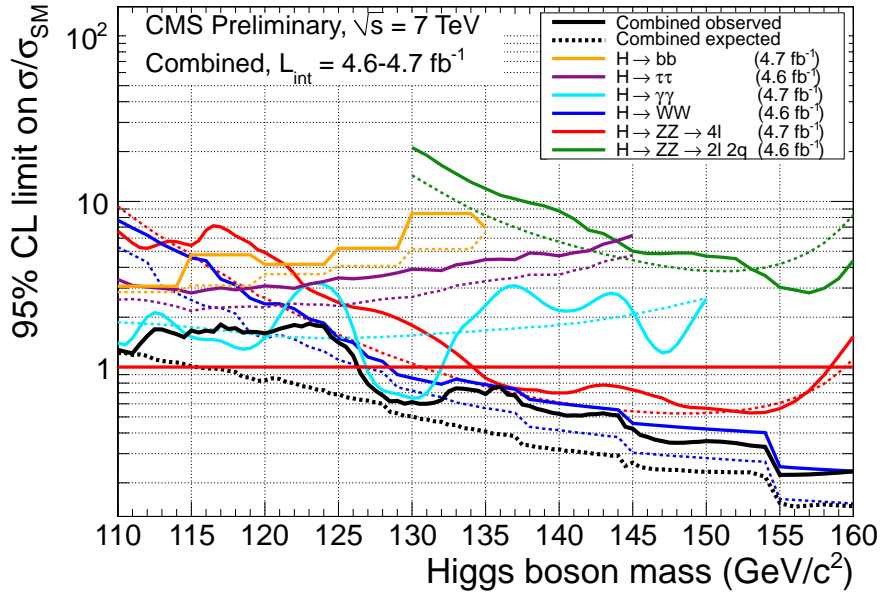


Figure 10: The observed and expected 95% C.L. upper limits on the signal strength modifier  $\mu = \sigma/\sigma_{\text{SM}}$  as a function of the SM Higgs boson mass for the six analyses used in the combination in the range 110–160  $\text{GeV}/c^2$ . Solid lines are for observed limits, dashed for expected.

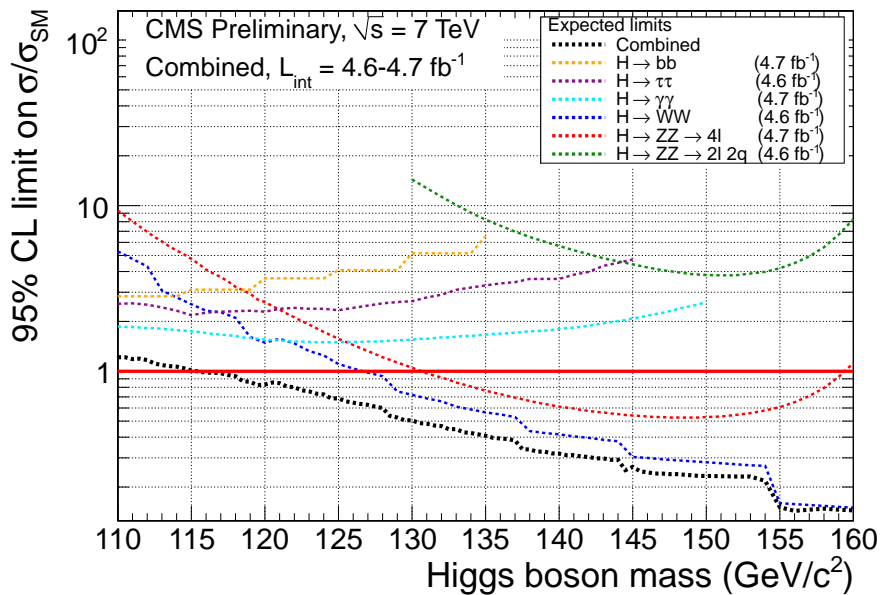


Figure 11: The expected 95% C.L. upper limits on the signal strength modifier  $\mu = \sigma/\sigma_{\text{SM}}$  as a function of the SM Higgs boson mass for the six analyses used in the combination in the range 110–160  $\text{GeV}/c^2$ .

## Anatomy of the excesses

Figures 12 and 13 (top panels) show a scan of the observed combined local  $p$ -value as given by Eq. (8) vs. Higgs boson mass  $m_H$ . This scan characterizes how unlikely are the upward departures in the observed values of the test statistic  $q_0^{obs}$ , under the background-only hypothesis.

One can see that the  $p$ -value curve dips downward over a broad range of low masses, driven by the broad excess seen in the  $WW$  analysis, with a few narrower features corresponding to the  $ZZ \rightarrow 4\ell$  events and modulations seen in the  $H \rightarrow \gamma\gamma$  channel. The first dip at  $m_H = 119 \text{ GeV}/c^2$  corresponds to three  $4\ell$  events with  $m_{4\ell} = 119 \text{ GeV}/c^2$ . The second dip is mostly driven by the  $\gamma\gamma$  excess around  $m_{\gamma\gamma} = 124 \text{ GeV}/c^2$ . The high mass dip at  $m_H = 325 \text{ GeV}/c^2$  corresponds to 9  $4\ell$  events in the mass range of 300–350  $\text{GeV}/c^2$ . The minimum local  $p$ -value is  $p_{min} = 0.005$  and corresponds to a local significance of  $Z_{max} = 2.6$ .

The best-fit  $\hat{\mu}$  values, also shown in Figs. 12 and 13 (lower panels), represent the factor by which the SM Higgs boson cross section has to be rescaled to agree with the data. The blue band corresponds to  $\pm 1\sigma$  error (statistical+systematic) on the value of  $\hat{\mu}$  as obtained in the asymptotic approximation from  $\Delta q_\mu = 1$ . One can see that the 119 and 124  $\text{GeV}/c^2$  excesses, giving  $\hat{\mu}$  values well within  $1\sigma$  of 1, are not inconsistent with the expected SM Higgs boson cross section, which is also true of the entire not yet excluded low mass range.

Figure 14 shows the interplay of contributing final states for Higgs boson hypotheses with  $m_H = 119.5, 124, 137, \text{ and } 144 \text{ GeV}/c^2$ , with the choice of mass points motivated by the features seen in Fig. 13. All four mass points do not show any strong statistical tension between the channels entering the combination, despite the differences in their  $p$ -values at these points as seen in Fig. 13. The relative size of the error bars for the different channels indicates their relative sensitivities. For the 119.5 and 124  $\text{GeV}/c^2$  mass points, the channels do not differ dramatically in their sensitivities, while for the 137 and 144  $\text{GeV}/c^2$  mass points, the  $WW$  and  $ZZ \rightarrow 4\ell$  channels are notably more sensitive than the others.

Fig. 15 compares the observed local  $p$ -value calculated in the asymptotic approximation as before (solid black line) and using pseudo-data (blue points). One can see that the asymptotic approximation indeed gives a fair assessment of  $p$ -values. The expected  $p$ -values at any given mass point, should a Standard Model Higgs boson exist at that same mass, are also shown in Fig. 15 with the dashed line.

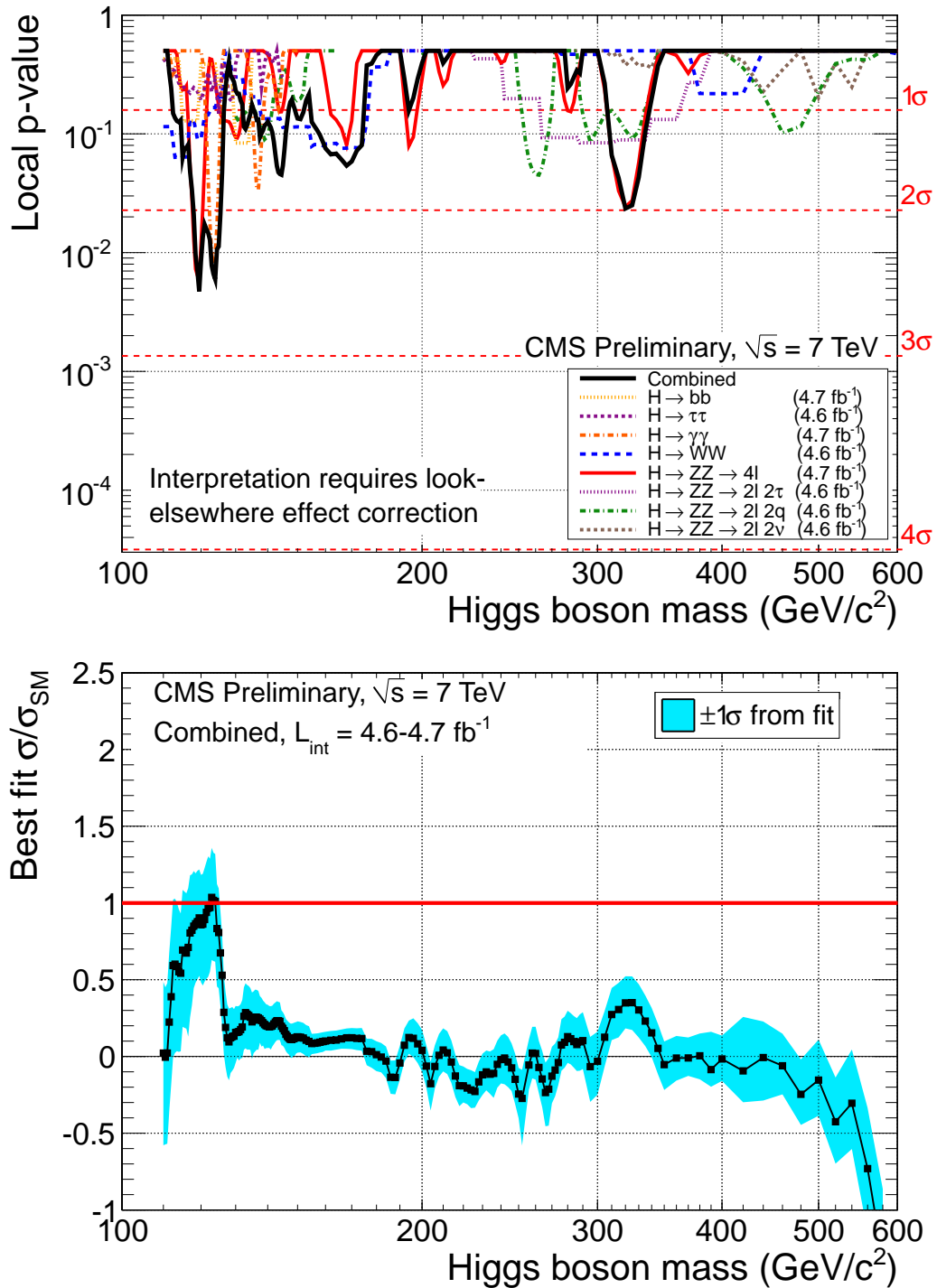


Figure 12: The observed local  $p$ -value  $p_0$  (top panel) and best-fit  $\hat{\mu} = \sigma/\sigma_{\text{SM}}$  (bottom panel) as a function of the SM Higgs boson mass in the range 110–600  $\text{GeV}/c^2$ . The solid black line on the plot of  $p$ -values is the combined result, while the coloured lines show results for individual channels.

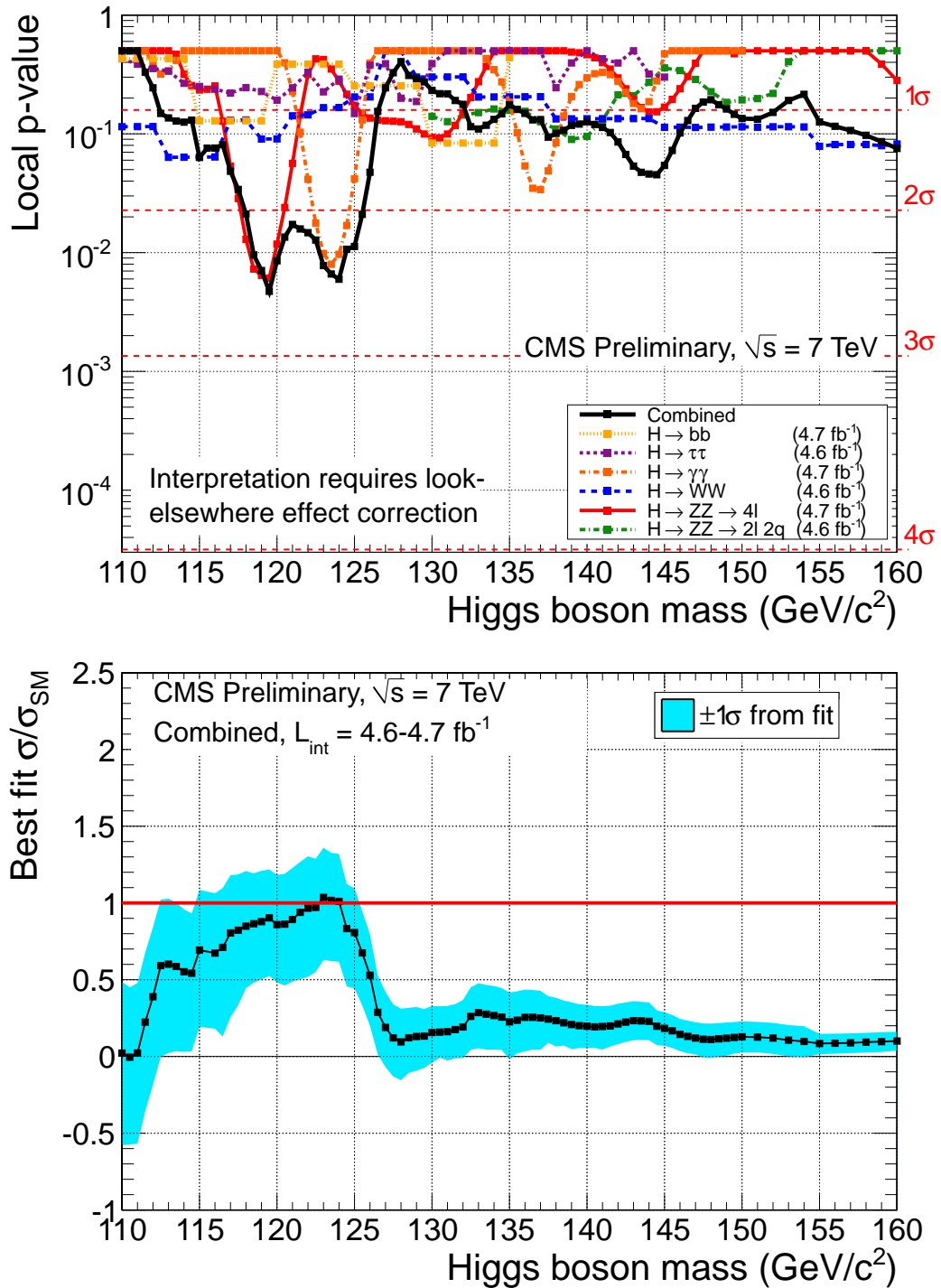


Figure 13: The observed local  $p$ -value  $p_0$  (top panel) and best-fit  $\hat{\mu} = \sigma/\sigma_{\text{SM}}$  (bottom panel) as a function of the SM Higgs boson mass in the range 110–160  $\text{GeV}/c^2$ . The solid black line on the plot of  $p$ -values is the combined result, while the coloured lines show results for individual channels.

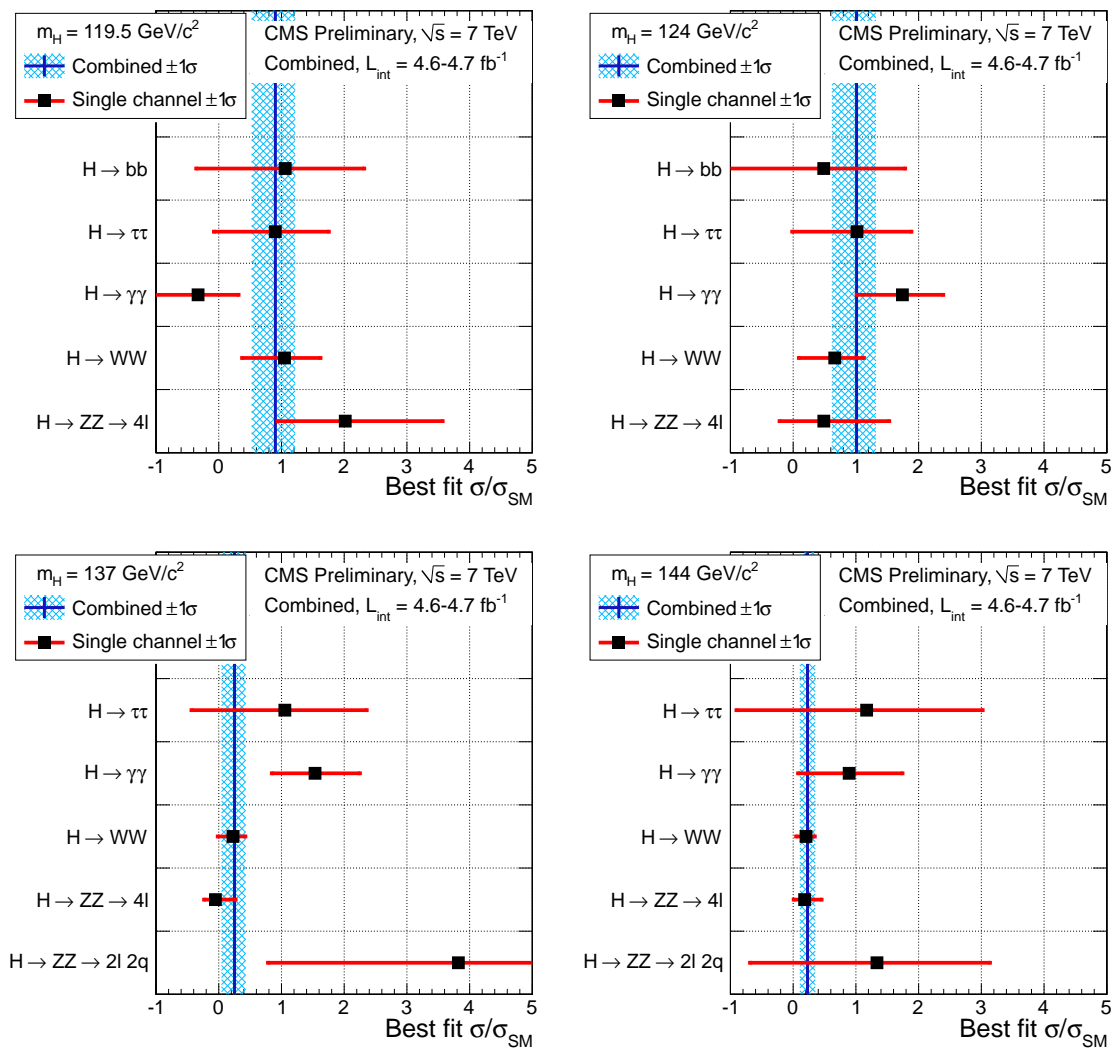


Figure 14: Values of  $\hat{\mu} = \sigma/\sigma_{SM}$  for the combination (solid vertical line) and contributing channels (points) for four hypothesized Higgs boson masses as indicated on the plot legends. The blue hatched band corresponds to the  $\pm 1\sigma$  errors on the overall  $\hat{\mu}$  value. The red horizontal bars indicate the  $\pm 1\sigma$  errors on the  $\hat{\mu}$  values for individual channels.

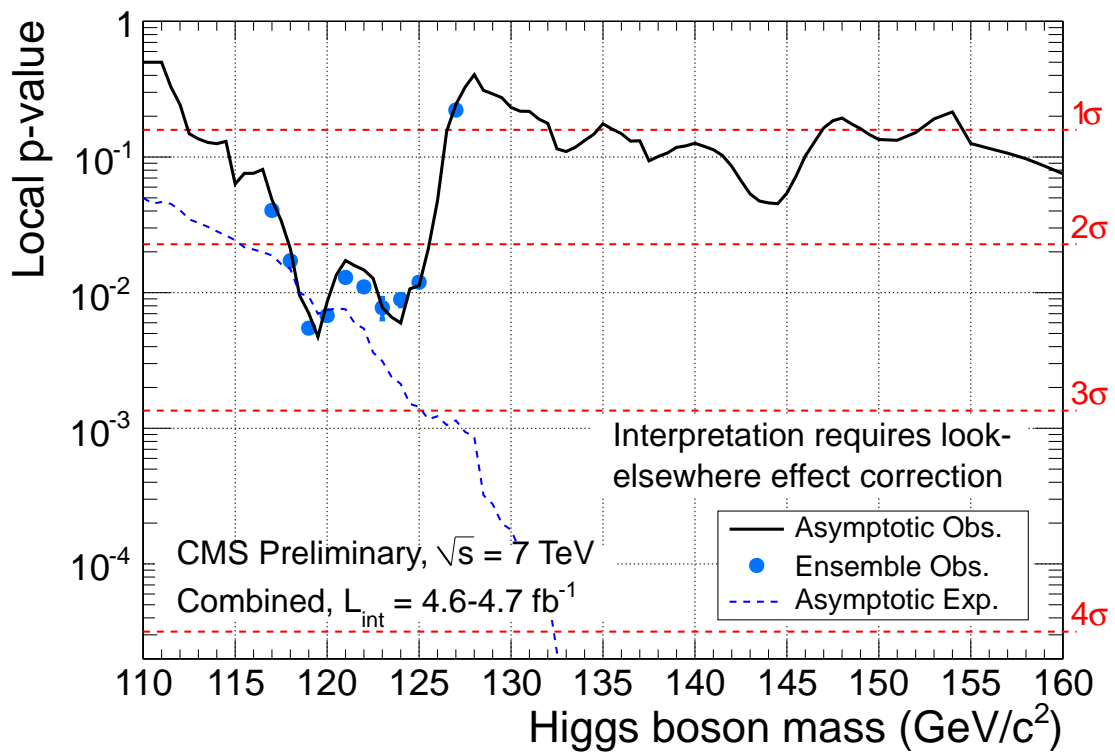


Figure 15: The observed local  $p$ -value  $p_0$  calculated in the asymptotic approximation (solid black line) and using pseudo-data (blue points). The expected  $p$ -values at any given mass point, should a Standard Model Higgs boson exist with that mass, are shown with the dashed line.

### Look-elsewhere effect in the full mass range

The look-elsewhere effect in this search is not negligible. For the *full search region*, 110-600 GeV/ $c^2$ , it can be approximately assessed by counting the number of deficit-to-excess fluctuations  $N_0$  across the entire search mass range as described in Ref [23]. The  $\hat{\mu}$  scan vs. Higgs boson mass (Fig. 12) shows 8 such upcrossings, where the  $\hat{\mu}(m_H)$  curve crosses  $\hat{\mu} = 0$  in a negative to positive direction. The global  $p$ -value to observe an excess with a local significance  $Z_{max} = 2.6$  is

$$p_{global} = p_{min} + N_0 e^{-Z_{max}^2/2} \sim 0.28,$$

which corresponds to a *global* significance of  $0.6\sigma$ .

### Look-elsewhere effect in the restricted mass range

Since the low-mass range is of particular interest in the SM Higgs boson search, we evaluate a look-elsewhere effect in the restricted mass range, chosen, by way of illustration, to be 110-145 GeV/ $c^2$ . To evaluate the *global*  $p$ -value in this mass range, we generate 500 pseudo-data sets for the background-only hypothesis and scan them for the minimum local  $p$ -value. The  $\gamma\gamma$ ,  $ZZ \rightarrow 4\ell$ , and  $\tau\tau$  pseudo-events are generated according to the relevant background models which are independent of the mass of the Higgs boson.

This cannot be done for the  $WW$  and  $bb$  analyses which use mass-dependent MVA-based techniques, preventing us from being able to build the necessary correlation models to correctly distribute pseudo-data events between MVAs trained for different mass points. However, by considering a narrow mass range, as we have done, we can take advantage of the fact that the  $WW$  and  $bb$  analyses have nearly no mass sensitivity. Therefore, for these channels we produce pseudo-data based on the background model obtained for a Higgs with mass,  $\tilde{m}_H$ , approximately at the mid-point of the restricted range. Signal models for other Higgs boson mass hypotheses are approximated by the model for  $\tilde{m}_H$ , with the total event yields adjusted according to the expected sensitivities obtained in the full analyses. By construction, the LEE trials factor for these channels becomes one, which is very close to the truth for so narrow a mass range.

Figure 16 shows the probability of observing a minimum *local*  $p$ -value equal or smaller than some predefined threshold. This probability is the *global*  $p$ -value. One can see that the *global*  $p$ -value corresponding to the observed  $p_{min} = 0.005$  is 0.026, which implies a *global* significance of  $1.9\sigma$ . An example of a  $p$ -value scan obtained in one of the 500 pseudo-data sets is shown in Fig. 17.

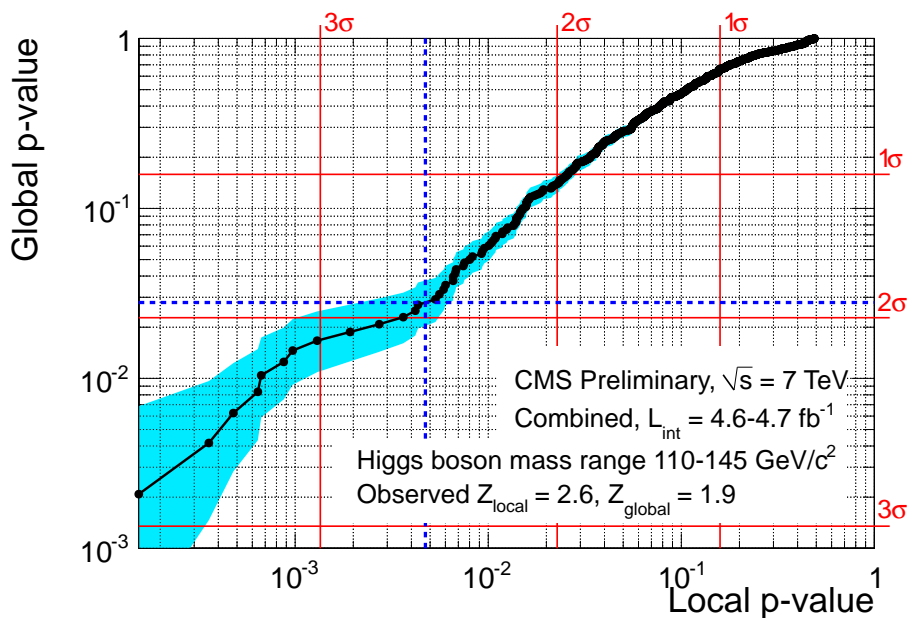


Figure 16: The global  $p$ -value to observe a minimum local  $p$ -value in the restricted mass range from 110–145  $\text{GeV}/c^2$ . The global  $p$ -value is assessed by generating pseudo-data.

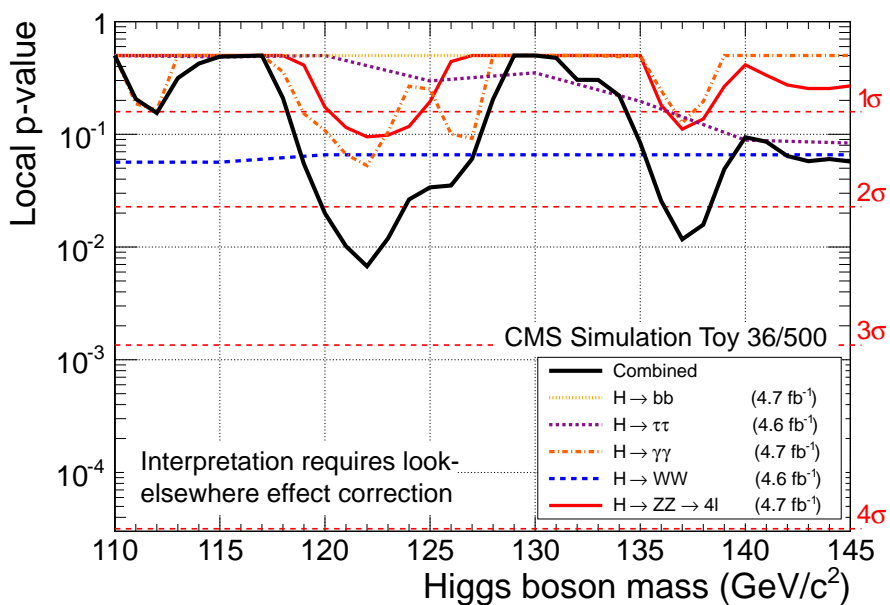


Figure 17: An example of a  $p$ -value scan obtained in one of the 500 pseudo-data sets.

### Sub-combinations in the low mass range

In this section, we combine the  $\gamma\gamma$  and  $4\ell$  channels which have a good mass resolution separately from the three channels with poor mass resolution,  $WW$ ,  $bb$ ,  $\tau\tau$ . The combination of the  $\gamma\gamma$  and  $4\ell$  analyses is shown in Figs. 18 and 19 (left), the  $WW$ ,  $bb$ , and  $\tau\tau$  combination—in Figs. 18 and 19 (right). Figure 20 is a summary plot of  $p$ -values for the two sub-combinations and the overall combined results.

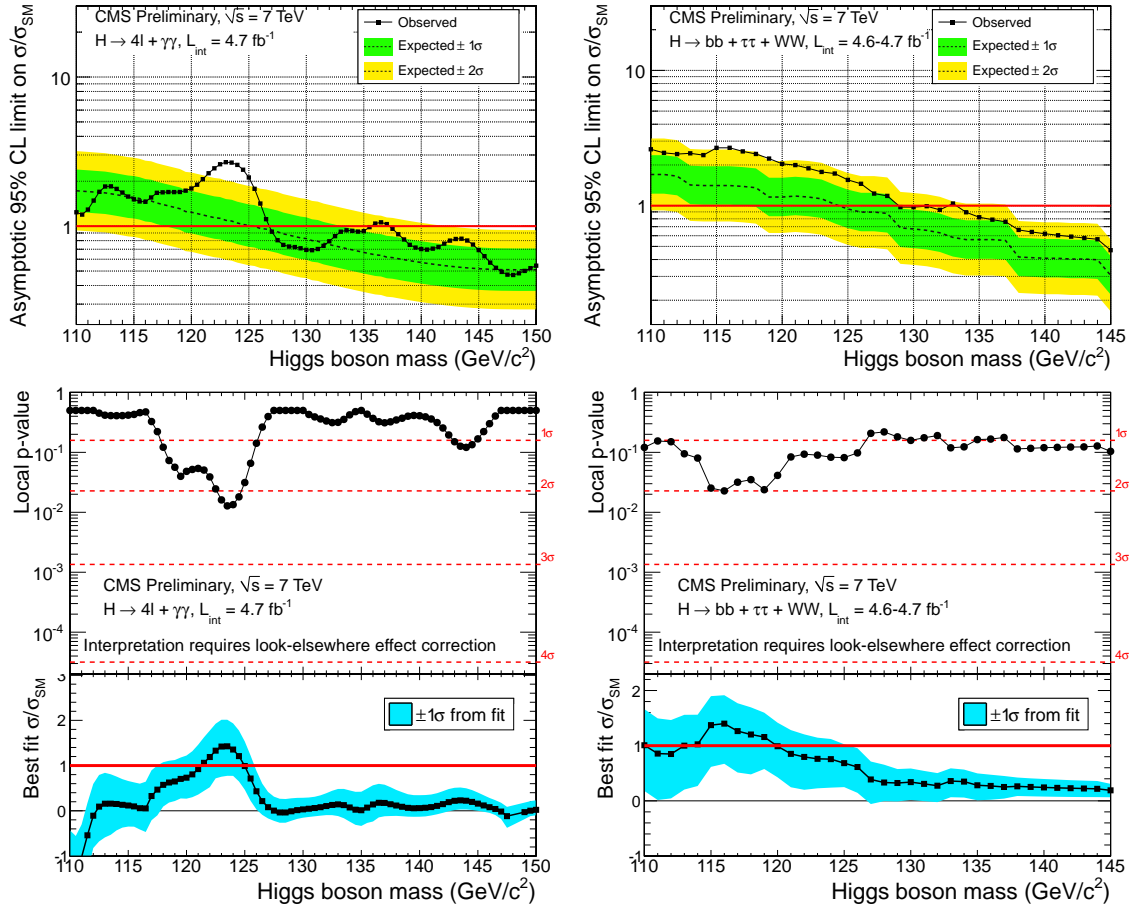


Figure 18: Exclusion limits on  $\mu$  (top), observed local  $p$ -value  $p_0$  and  $\hat{\mu}$  scans (bottom), for the combination of the  $\gamma\gamma$  and  $4\ell$  analyses (left) and the  $WW$ ,  $bb$ , and  $\tau\tau$  analyses (right).

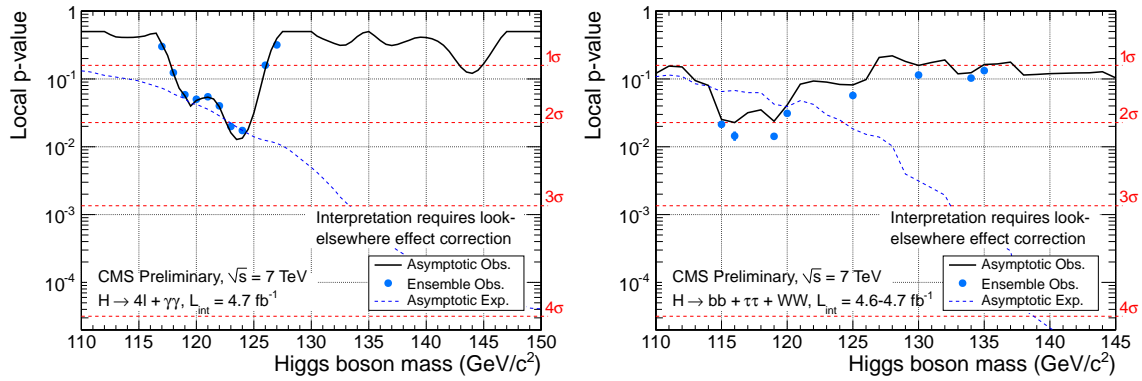


Figure 19: Observed and expected local  $p$ -values  $p_0$  for the combination of the  $\gamma\gamma$  and  $4\ell$  analyses (left) and the  $WW$ ,  $bb$ , and  $\tau\tau$  analyses (right).

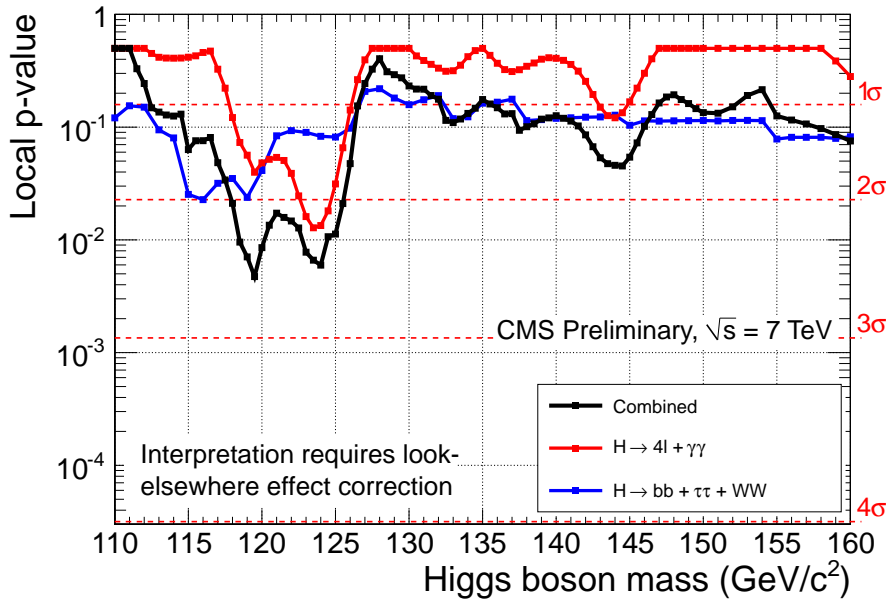


Figure 20: Observed local  $p$ -values  $p_0$  for the sub-combinations  $\gamma\gamma + 4\ell$  and  $WW + bb + \tau\tau$  and for the grand combination.

## Comparisons to Tevatron and LEP

Figures 21 and 22 show the limits on the SM Higgs boson mass as obtained by CMS in this combination overlaid with limits from LEP and Tevatron.

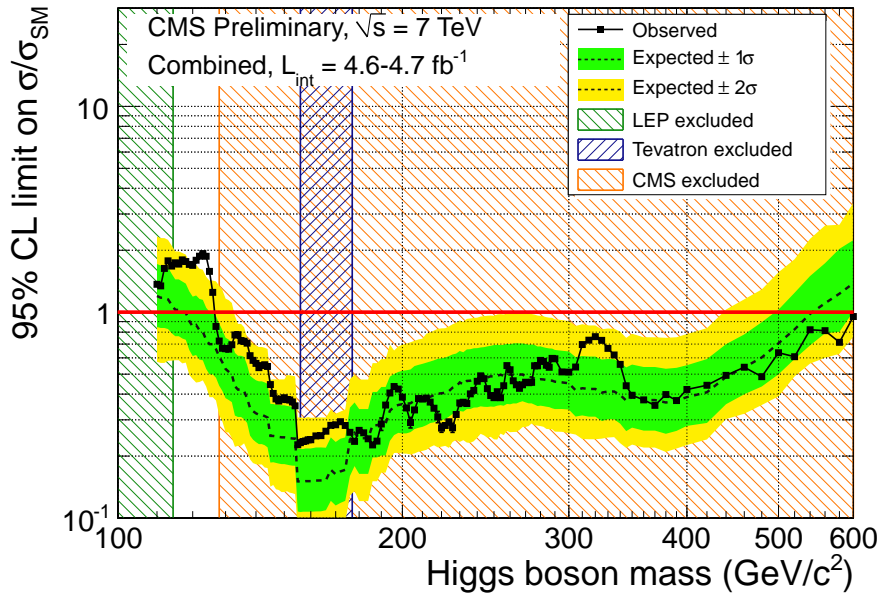


Figure 21: Higgs boson masses excluded by CMS, Tevatron, and LEP.

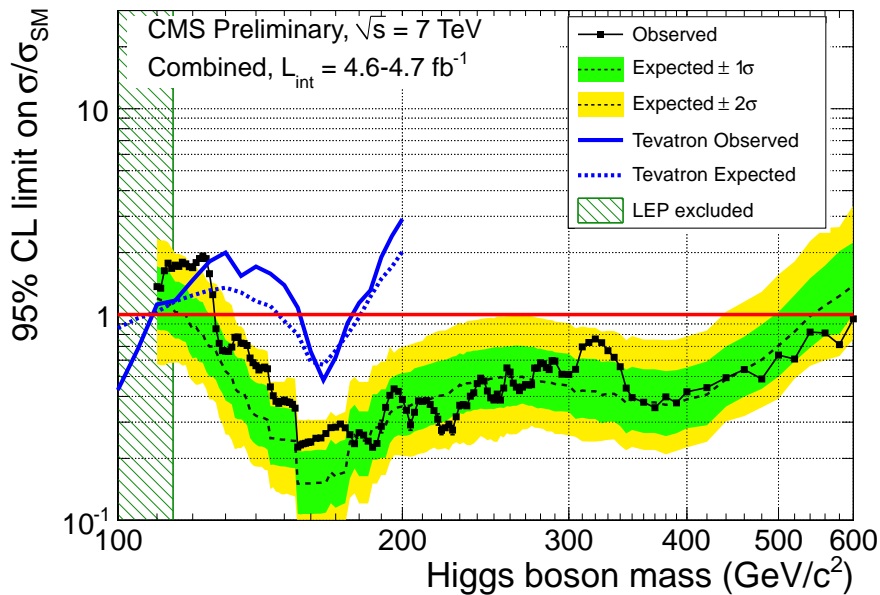


Figure 22: Expected and observed exclusion limits from CMS and Tevatron.

## References

- [1] F. Englert and R. Brout, "Broken symmetry and the mass of gauge vector mesons", *Phys. Rev. Lett.* **13** (1964) 321–323. doi:10.1103/PhysRevLett.13.321.
- [2] P. Higgs, "Broken symmetries, massless particles and gauge fields", *Phys. Lett.* **12** (1964) 132–133. doi:10.1016/0031-9163(64)91136-9.
- [3] P. Higgs, "Broken symmetries and the masses of gauge bosons", *Phys. Rev. Lett.* **13** (1964) 508–509. doi:10.1103/PhysRevLett.13.508.
- [4] G. Guralnik, C. Hagen, and T. Kibble, "Global conservation laws and massless particles", *Phys. Rev. Lett.* **13** (1964) 585–587. doi:10.1103/PhysRevLett.13.585.
- [5] P. Higgs, "Spontaneous symmetry breakdown without massless bosons", *Phys. Rev.* **145** (1966) 1156–1163. doi:10.1103/PhysRev.145.1156.
- [6] T. Kibble, "Symmetry breaking in non-Abelian gauge theories", *Phys. Rev.* **155** (1967) 1554–1561. doi:10.1103/PhysRev.155.1554.
- [7] R. Barate and others (LEP Working Group for Higgs boson searches and ALEPH, DELPHI, L3, and OPAL Collaborations), "Search for the standard model Higgs boson at LEP", *Phys. Lett.* **B565** (2003) 61–75, arXiv:hep-ex/0306033. doi:10.1016/S0370-2693(03)00614-2.
- [8] CDF and D0 Collaborations, "Combined CDF and D0 upper limits on Standard Model Higgs Boson production", (July, 2011). arXiv:1107.5518. CDF Note 10606 and D0 Note 6226.
- [9] ATLAS and CMS Collaborations, "Combined Standard Model Higgs boson searches with up to  $2.3 \text{ fb}^{-1}$  of pp collision data at  $\sqrt{s} = 7 \text{ TeV}$  at the LHC", (November, 2011). ATLAS-CONF-2011-157, CMS HIG-11-023.
- [10] The ALEPH, CDF, D0, DELPHI, L3, OPAL, SLD Collaborations, the LEP Electroweak Working Group, the Tevatron Electroweak Working Group, and the SLD electroweak and heavy flavour groups, "Precision Electroweak Measurements and Constraints on the Standard Model", (December, 2010). CERN-PH-EP-2010-095, arXiv:hep-ex/1012.2367v2. NOTE: The Higgs boson mass limit is  $m_H < 161 \text{ GeV}/c^2$ , according to the July 2011 undocumented update.
- [11] CMS Collaboration, "The CMS experiment at the CERN LHC", *JINST* **3** (2008) S08004. doi:10.1088/1748-0221/3/08/S08004.
- [12] LHC Higgs Cross Section Working Group, S. Dittmaier, C. Mariotti et al., "Handbook of LHC Higgs Cross Sections: 1. Inclusive Observables", CERN-2011-002 (CERN, Geneva, 2011) arXiv:1101.0593.
- [13] CMS Collaboration, "Search for a Higgs boson decaying into two photons in the CMS detector", *CMS PAS HIG-11-030* (2011).
- [14] CMS Collaboration, "Search for the Standard Model Higgs Boson decaying to Bottom Quarks and Produced in Association with a W or a Z Boson", *CMS PAS HIG-11-031* (2011).

- [15] CMS Collaboration, “Search for Neutral Higgs Bosons Decaying to Tau Pairs in pp Collisions at  $\sqrt{s} = 7$  TeV”, *CMS PAS HIG-11-029* (2011).
- [16] CMS Collaboration, “Search for the Higgs Boson Decaying to  $W^+W^-$  in the Fully Leptonic Final State”, *CMS PAS HIG-11-024* (2011).
- [17] CMS Collaboration, “Search for a Standard Model Higgs boson produced in the decay channel  $H \rightarrow ZZ^{(*)} \rightarrow 4\ell$ ”, *CMS PAS HIG-11-025* (2011).
- [18] CMS Collaboration, “Search for a standard model Higgs boson produced in the  $H \rightarrow ZZ \rightarrow \ell^+\ell^-\tau^+\tau^-$  decay channel with CMS detector at  $\sqrt{s} = 7$  TeV”, *CMS PAS HIG-11-028* (2011).
- [19] CMS Collaboration, “Search for the Higgs boson in the  $H \rightarrow ZZ \rightarrow 2\ell 2\nu$  channel in pp collisions at  $\sqrt{s} = 7$  TeV”, *CMS PAS HIG-11-026* (2011).
- [20] CMS Collaboration, “Search for the standard model Higgs Boson in the decay channel  $H \rightarrow ZZ \rightarrow q\bar{q}\ell^-\ell^+$  at CMS”, *CMS PAS HIG-11-027* (2011).
- [21] T. Junk, “Confidence level computation for combining searches with small statistics”, *Nucl.Instrum.Meth.* **A434** (1999) 435–443, arXiv:hep-ex/9902006.  
doi:10.1016/S0168-9002(99)00498-2.
- [22] A. L. Read, “Modified frequentist analysis of search results (the CLs method)”, *CERN Yellow Report CERN-2000-005* (2000) 81.
- [23] ATLAS Collaboration, CMS Collaboration, and LHC Higgs Combination Group, “Procedure for the LHC Higgs boson search combination in summer 2011”, *ATL-PHYS-PUB-2011-818*, *CMS NOTE-2011/005* (August, 2011).
- [24] G. Cowan, K. Cranmer, E. Gross and O. Vitells, “Asymptotic formulae for likelihood-based tests of new physics”, *Eur. Phys. J.* **C71** (2011) 1–19.
- [25] E. Gross and O. Vitells, “Trial factors for the look elsewhere effect in high energy physics”, *The European Physical Journal C - Particles and Fields* **70** (2010) 525–530.
- [26] A. O’Hagan and J.J. Forster, “Kendall’s Advanced Theory of Statistics. Vol. 2B: Bayesian Inference”. Arnold, London, 2004.